Contents lists available at SciVerse ScienceDirect

Comptes Rendus Chimie

www.sciencedirect.com

Full paper/Mémoire

Biocompatible nanoparticles and gadolinium complexes for MRI applications

Thomas Courant [a,b], Gaelle V. Roullin [a], Cyril Cadiou [b], Maité Callewaert [a], Marie C. Andry [a], Christophe Portefaix [c], Christine Hoeffel [c], Marie C. de Goltstein [d], Marc Port [d], Sophie Laurent [e], Luce Vander Elst [e], Robert N. Muller [e,f], Michael Molinari [g], Françoise Chuburu [b,*]

[a] Institut de chimie moléculaire de Reims, CNRS UMR 7312, UFR Pharmacie Reims, 51, rue Cognacq-Jay, 51100 Reims, France
[b] Institut de chimie moléculaire de Reims, CNRS UMR 7312, UFR des sciences exactes et naturelles, bâtiment 18, Europol'Agro, BP 1039, 51687 Reims cedex 2, France
[c] CHU de Reims, Service de radiologie, hôpital Maison-Blanche, 45, rue Cognacq-Jay, 51092 Reims cedex, France
[d] GUERBET, BP57400, 95943 Roissy-Charles-de-Gaulle cedex, France
[e] NMR and Molecular Imaging Laboratory, Department of General, Organic and Biomedical Chemistry, University of Mons, 19, avenue Maistriau, 7000 Mons, Belgium
[f] Center for Microscopy and Molecular Imaging, 8, rue Adrienne-Bolland, 6041 Charleroi, Belgium
[g] Laboratoire de recherche en nanosciences, UFR des Sciences, université de Reims–Champagne-Ardenne, 21, rue Clément-Ader, 51685 Reims cedex 2, France

ARTICLE INFO

ABSTRACT

Performances of double-emulsion techniques (W/O/W and W/O/O) and ionotropic gelation process were compared to achieve encapsulation of gadolinium MRI contrast agents (GdCAs) into biocompatible polymeric nanoparticles (NPs) with high Gd-loadings. The better approach proved to be ionotropic gelation with H[Gd(DOTA)] as GdCA. Relaxometry evaluation of H[Gd(DOTA)]⊂NPs efficiency demonstrated that incorporation of H[Gd(DOTA)] inside an hydrogel matrix highly improved H[Gd(DOTA)] relaxivity. Particle efficacy as MR contrast agents was further demonstrated on a 3 T clinical imager: a significant improvement of T_1- and T_2- MR signals was obtained at doses much lower than the currently used.

© 2012 Académie des sciences. Published by Elsevier Masson SAS. All rights reserved.

RÉSUMÉ

L'encapsulation d'agents de contraste IRM à base de gadolinium (GdCAs) dans des nanoparticules (NPs) polymères biocompatibles a été réalisée par double émulsion (W/O/W et W/O/O) et gélation ionique. La gélation ionique s'avère la meilleure stratégie en présence de H[Gd(DOTA)]. L'évaluation relaxométrique des H[Gd(DOTA)]⊂NPs montre que l'incorporation de cet agent dans une matrice hydrogel exalte sa relaxivité. L'efficacité de ces NPs comme agents de contraste pour l'IRM est mise en évidence sur un imageur clinique 3 T : une amélioration significative des signaux en modes T_1 et T_2 est observée pour des doses bien plus faibles que ce qui est actuellement administré.

© 2012 Académie des sciences. Publié par Elsevier Masson SAS. Tous droits réservés.

1. Introduction

Magnetic resonance imaging (MRI) is a routinely used non-invasive diagnostic tool providing high-resolution anatomical images (sub-millimeter spatial resolution).

Physical principles of MRI rely on the relaxation of water protons, which depends on the magnetic fields (the strong static magnetic field B_0 and the radiofrequency field), on the pulse sequence, and on the heterogeneous distribution and environment of water in the organism [1]. Indeed, variations of proton longitudinal (T_1) and transversal (T_2) magnetic relaxation times are partly responsible for the image contrast [1]. However, in some examinations, the

* Corresponding author.
  E-mail addresses: gaelle.roullin@univ-reims.fr (G.V. Roullin), francoise.chuburu@univ-reims.fr (F. Chuburu).

information obtained from a simple MR image is not sufficient to highlight areas of interest. Thus, the contrast has to be improved, by administering optimal contrast-enhancing agents (CAs). The most currently used contrast agents are T_1-CAs, constituted of paramagnetic complexes of metal ions with symmetrical electronic ground states, such as gadolinium (GdCAs) [1,2]. Paramagnetic T_1-CAs predominantly shorten the longitudinal relaxation times of water protons in their vicinity. This effect gives rise to signal intensity increase (positive CAs) and then to a better differentiation between healthy and pathological tissues. GdCA efficiency is defined by its relaxivity r_i (mM^{-1} s^{-1}), which corresponds to selective reduction of the relaxation times of the water protons brought about by a 1 mM concentration of paramagnetic centers. To improve this efficacy, the Solomon-Bloembergen-Morgan theory [3] establishes outlines to design more efficient contrast agents [4]. For applications at 0.5–1.5 T, relaxivity improvement per Gd center can be achieved by high Gd-loadings and by controlling the tumbling motion of the GdCAs, through association of metal complexes to macro- or supramolecular carriers [5]. Another way to insure reduced tumbling rates, and larger payloads of active magnetic centers, is to graft or to encapsulate them into nanoparticles (NPs). Different nanoplatforms such as viral capsules, lipoprotein or apoferritin, [5] as well as liposomal NPs, [2b] micelles, [2b] Nanoscale Metal-Organic-Frameworks, [6] fullerenes [7] and inorganic NPs [8] have been used. However, the biocompatibility of these objects is a crucial factor whenever in vivo applications are implied. In this respect, polymeric biocompatible NPs are ideal candidates for the vectorization of contrast agents.

To improve MRI GdCA efficiency, our purpose was then to encapsulate some currently marketed contrast agents into a biocompatible matrix, by using a fully biocompatible protocol. Since GdCAs are highly hydrophilic chelates, the challenge was to achieve high Gd-loadings inside the NP framework. Recently, we have demonstrated that hydrophilic copper complexes, homologous to GdDOTA, can be satisfactorily incorporated in PLGA (Poly[D, ʟ-lactide-co-glycolide]) nanoparticles through a double-emulsion technique [9]. In this paper, we demonstrate, via several adaptations of the double-emulsion technique, that this methodology is not appropriate for GdCAs. We also compare these attempts to an alternative protocol recently published, based on a ionotropic gelation process which involves hydrophilic biopolymers [10]. For each protocol, encapsulation of a set of GdCAs was attempted. Systematic evaluation of NP morphologies, GdCA encapsulation efficiencies, as well as NP production yields allowed to select the best combination between polymer matrix and Gd contrast agents. For the optimal condition, relaxation rate measurements ($1/T_1$ and $1/T_2$) at 20 and 60 MHz were performed.

2. Experimental

2.1. General

All chemicals were used as received without further purification. Solvents were of pharmaceutical grade. Poly(D, ʟ-lactide-co-glycolide) (PLGA, 50:50 lactide/glycolide) was purchased from Sigma–Aldrich, France. Sodium hyaluronate was extracted from Streptococcus equi sp. (Sigma-Aldrich, France). Chitosan (low-molecular weight) was purchased from Sigma (France). Poloxamer 188 (Pluronic® F-68, polyethyleneglycol-co-polypropyleneglycol-copolyethyleneglycol) was purchased from Sigma-Aldrich, France. Lipoid® S75 was purchased from Lipoid GMBH (Germany). Stelliesters® was kindly donated by Stéarinierie Dubois (France). 1,2,3-Triacetoxypropane (triacetin) was purchased from Sigma–Aldrich, France. Ninety-five percent (v/v) ethanol was obtained from Charbonneaux Brabant (France). Sterile water for injections (Aqua B. Braun, Melsungen, Germany) was systematically used for nanoparticle preparation and analysis.

Gd-CAs used in this study were commercially available (Dotarem®, Guerbet, France; Multihance®, Bracco Imaging, France; Prohance®, Bracco Imaging, France; Magnevist®, Bayer Santé, France).

2.2. Nanoparticle syntheses

2.2.1. W/O/W double-emulsion protocol

2.2.1.1. Basic protocol. The formation of Gd-CA loaded nanoparticles was achieved by adjusting the multiple emulsion technique, i.e. water (internal, Wi)-in-oil (O)-in water (external, We) previously described for Cu-complex encapsulation [9]. Briefly, 750 μL of aqueous triacetin-saturated phase Wi consisting of the chosen Gd-CAs ($\sim 5 \times 10^{-5}$ mol) and Poloxamer P188 0.1% w/v, pH = 10 was emulsified in an organic phase O of PLGA 3% w/v in 5 mL triacetin, under ultrasonic stirring (Vibracel VC 750, $\sim$ 20–25 °C, 30 s, 22%). Then, 10 mL of an aqueous triacetin-saturated solution containing the same percentage of Poloxamer P188 were added to this primary emulsion to obtain the double-emulsion (Wi/O/We). Afterwards, the droplets were converted into nanoparticles through the solvent diffusion step, carried out with addition of 150 mL of ethanol. Raw nanoparticle suspensions were obtained within 0.5 h.

2.2.1.2. Alternative strategy 1. An alternative protocol was used by replacing Poloxamer P188 by Tween® 20, 5% w/v in all aqueous phases, while maintaining all other parameters identical.

2.2.1.3. Alternative strategy 2. A second alternate strategy was used by replacing the organic phase O by one containing PLGA dissolved in triacetin, added with various amounts of Poloxamer P188 (0.75, 1.5 or 3% w/v). All other parameters were kept constant.

2.2.2. W/O/O double-emulsion protocol

Gd-CA loaded nanoparticles could also be prepared by a totally biocompatible multiple emulsion technique water (W)-in-oil (O_1)-in-oil (O_2). Briefly, 750 μL of aqueous triacetin-saturated phase Wi consisting of the chosen Gd-CAs ($\sim 5 \times 10^{-5}$ mol) and Tween® 20, 5% w/v, pH = 10 was emulsified in an organic phase O of PLGA 3% w/v in 5 mL triacetin, under ultrasonic stirring (Vibracel VC 750, $\sim$ 20–25 °C, 30 s, 22%). Then, 10 mL of an organic solution O_2

containing Lipoid® S75 1% w/v dissolved in Stelliesters® were added to this primary emulsion to obtain the double-emulsion (W/O$_1$/O$_2$). Afterwards, the droplets were converted into nanoparticles through the solvent diffusion step, carried out with addition of 150 mL of ethanol. Raw nanoparticle suspensions were obtained within 0.5 h.

2.2.3. Ionotropic gelation protocol

Chitosan (22.5 mg) was added to a solution of citric acid [10% (w/v), 9 mL, pH = 2] and magnetically stirred for 2 h until complete dissolution. [10] The chosen Gd-CA ($\sim 2.5 \times 10^{-5}$ mol) was then added to the acidic chitosan solution and magnetic stirring was maintained for 10 min. A solution of sodium tripolyphosphate (5.4 mg; 14.7 μmol) and sodium hyaluronate (3.6 mg) in water (4.5 mL) was then added dropwise under constant magnetic stirring. At the end of addition, stirring was maintained for another 10 min. The solution changed from colorless to turbid (characteristic Tyndall Effect).

2.3. Nanoparticle purification

The raw nanoparticle suspensions (10 mL) were usually purified from free GdCAs and excess solvent and tensioactive molecules by being dialyzed three times at room temperature against 2.0 L of water for injections, for 24 h with magnetic stirring (Spectra/Por® 6.0, MWCO 25 kDa, Spectrum Laboratories, USA).

2.4. Nanoparticle characterization

2.4.1. Particle size analysis and zeta-potential measurements

Dynamic light scattering (DLS) was used for measurement of average hydrodynamic diameters (D_h) and polydispersity indexes (PdIs) (Malvern Zetasizer Nano-ZS, Malvern Instruments, Worcestershire, UK). Each sample was analyzed in triplicate at 20 °C at a scattering angle of 173°. Pure water was used as a reference-dispersing medium. DLS data were always expressed in % intensity in order to detect the potential presence of aggregates in the nanoparticle suspensions.

ζ-(zeta) potential data were collected through electrophoretic light scattering at 20 °C, 150 V, in triplicate for each sample (Malvern Zetasizer Nano-ZS). The instrument was calibrated with a Malvern – 68 mV standard before each analysis cycle.

2.4.2. Morphological studies – AFM images

The shape and the surface morphology of the NPs were investigated by atomic force microscopy (AFM). Samples were prepared by placing a drop of nanoparticle suspension on a freshly cleaved mica sheet and allowing it to dry in air. AFM imaging was performed using a Nanoscope V (Brüker Nano) in tapping mode. A silicon tip with a spring constant of 46 N/m and a resonance frequency around 300 kHz were used. AFM images were generated with a scan rate of 1 Hz and 512 lines per image. Experiments were performed at constant room temperature. During the scans, proportional and integral gains were increased to the value just below the feedback started to oscillate. Images were processed only by flattening to remove background slopes.

2.4.3. Nanoparticle elemental composition by TEM–EDXS

A scanning transmission electron microscope (CM30, Philips, Limeil-Brevannes, France) equipped with an EDAX 30 mm^2 Si(Li) R-SUTW detector was used for determining elemental composition of nanoparticles. In practice, a drop of NP suspension was deposited on a 200-mesh copper grid covered by a collodion/carbon film and X-ray spectra were acquired for 100 s at 100 keV by a 24-nm probe focalized on the nanoparticles. The emission spectrum corresponds to the counting of X-rays emitted according to their energy.

2.4.4. Gadolinium loadings

Gadolinium nanoparticle loadings were determined on NP suspensions by ICP-AES. The non-encapsulated complexes were separated from the NPs by high-speed centrifugation for 1 h at 4 °C at 23,200 g (Beckman Avanti™ J-E Centrifuge, France). The NP pellet was then incubated in H$_2$SO$_4$ 2 mol/L for 48 h at 45 °C. After the NP destruction, volumetric dilutions were carried out to achieve an approximate Gd concentration within the working range of the method. Counts of Gd were correlated to a Gd concentration based on a standard generated by mixing Gd(NO$_3$)$_3$ with unloaded NPs incubated under the same acidic conditions.

Gadolinium complexes entrapment efficiency (EE,%) was calculated by Eq. (1)

$$EE = \frac{mass\ of\ Gd\ complex\ in\ particles}{mass\ of\ Gd\ complex\ used\ in\ formulation} \times 100 \tag{1}$$

The final number of chelates per NP (Y_{Gd}) was estimated as described in ref [9].

2.5. T_1 and T_2 measurements at 20 MHz (0.47 T) and 60 MHz (1.5 T)

T_1 and T_2 measurements were performed on Bruker mq20 and Bruker mq60 Minispec relaxometers. T_1 and T_2 were determined at 20 MHz (0.47 T) and 60 MHz (1.5 T) using an inversion recovery pulse sequence. Temperature was equilibrated and maintained at 37 °C during the scans. Each sample was analyzed by ICP-AES to take into account the exact Gd concentration. The inverse of the paramagnetic longitudinal relaxation time ($1/T_{1\ para}$, s^{-1}) and paramagnetic transversal relaxation time ($1/T_{2\ para}$, s^{-1}) of each sample were plotted against Gd(III) concentration (mM) and fitted using linear regression ($R^2 > 0.99$).

Finally, $(1/T_{i\ para}) = (1/T_{i\ observed}) - (1/T_{i\ dia})$.

2.6. MR imaging

MR imaging of NP suspensions were performed by using a 3.0 T MRI device (Achieva, Philips Medical Systems, The Netherlands) with a Sense head 8-channel coil. T_1-weighted images were obtained using an axial spin echo T_1 sequence (TR = 160 ms, TE = 8 ms, FOV = 170 × 170 mm, matrix = 192 × 192, slice thickness = 2 mm, acquisition number = 1). T_2-weighted images were obtained with an axial turbo spin echo T_2
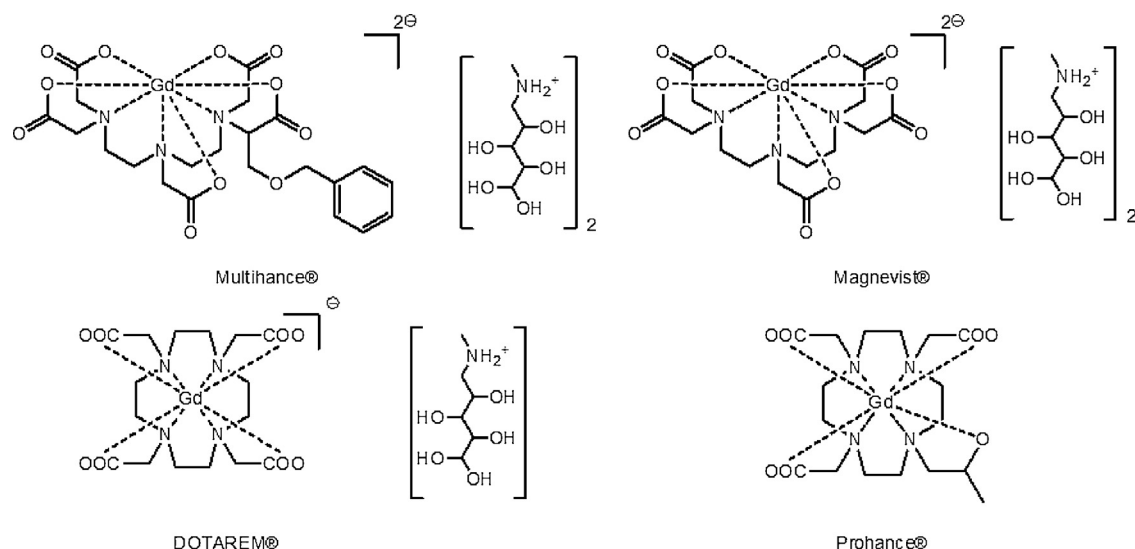
Scheme 1. GdCAs under study.
Scheme 1. GdCAs étudiés.

(TSE multishot) sequence (TR = 5000 ms, TE = 80 ms, FOV = 100 × 100 mm, matrix = 256 × 256, slice thickness = 2 mm, acquisition number = 1).

3. Results and discussion

Three currently marketed contrast agents Multihance®, DOTAREM® and Prohance® together with sodium salt of DOTAREM® [Na(Gd(DOTA)] (GdCAs, Scheme 1) were encapsulated in the pre-formed poly(D, L-lactide-co-glycolide) polymer (PLGA 50:50) by a bottom-up approach. These Gd-chelates were chosen in order to test whether their charge and/or the counter-ion nature (meglumine cation in commercial formulations see Scheme 1, or sodium cation for [Na(Gd(DOTA))] could influence the encapsulation efficiency.

As demonstrated by their negative log P value (measured between butanol and water, Table 1) [11], these complexes are characterized by a pronounced hydrophilicity, reinforced by their ionic charge.

Consequently, encapsulation of these hydrophilic agents inside PLGA matrix (which is rather hydrophobic) was firstly performed via the dedicated water-in-oil-in-water (Wi/O/We) double-emulsion, under a high energy emulsification process [9]. The choice of this technique was guided by previous successful encapsulation of a

copper analog of DOTA for which high metal loadings were achieved. In this procedure, the emulsion is composed of aqueous droplets containing GdCAs, which are dispersed inside oily drops, these oily drops being themselves dispersed in an external aqueous phase (Fig. 1a) [12,13].

The biocompatibility of the process was ensured by the use of pharmaceutically-accepted excipients, triacetin [14] as the organic solvent and poly(ethyleneglycol)$_{30}$-co-poly(propyleneglycol)$_{75}$-co-(polyethyleneglycol)$_{30}$ (Poloxamer 188) [14] as the tensioactive. Diffusion of triacetin in EtOH 95% provoked polymer chain desolvation and thus W/O/W droplets solidification as NPs. Finally, the resulting raw nanoparticles were quasi-quantitatively recovered (NP production yield ∼ 95%), purified by dialysis, morphologically characterized by DLS/ELS analyses and the encapsulation efficiency [EE, equation (1)] determined by ICP-AES titrations (Table 2). DLS analysis indicated that NPs were narrowly monodisperse (polydispersity index inferior to 0.1) with mean diameters compatible with medical applications (within the 250 nm range). ξ-potentials, strongly negative, contributed to the final colloidal suspension stability.

Encapsulation efficiency (EE) can be seen as the yield of Gd-chelate encapsulation. The values determined through ICP-AES titrations were inferior to 1% whatever the GdCA. This result showed that differences in hydrophilicity and counter-anion had no impact on the GdCA encapsulation. Nevertheless, these EE values were very low and the majority of the introduced complex was recovered outside the NPs at the end of the synthesis. These results were unexpected since, for analog copper complexes (of similar hydrophilicity and ionic charge), EE values between 13 and 28% and consequent high NP Cu loadings are reached [9]. They could be interpreted by the destabilization of the emulsion, mainly due to the migration and/or destruction of aqueous droplets containing GdCAs [15]. To prevent this destabilization, several strategies were considered in order

Table 1
Principal characteristics of GdCAs under study.
Tableau 1
Principales caractéristiques des GdCAs étudiés.

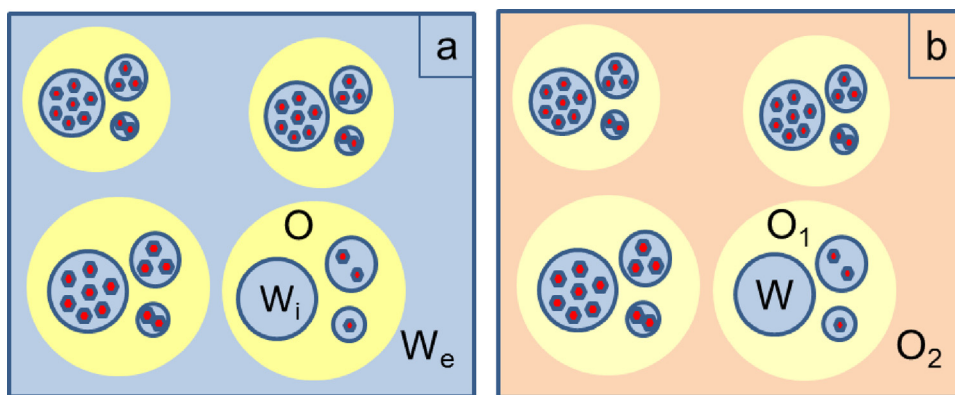| GdCAs	Chemical structure	log P (BuOH/H$_2$O) [11]	Charge
DOTAREM®	Macrocyclic	−2.87	−1
Prohance®	Macrocyclic	−1.98	0
Multihance®	Linear	−2.33	−2

Fig. 1. Schematic representations of (a) water-in-oil-in-water, (b) water-in-oil-in-oil emulsions (● = GdCA).

Fig. 1. Représentations schématiques des double émulsions (a) eau-dans-huile-dans-eau (W/O/W), (b) eau-dans-huile-dans-huile (W/O/O) (● = GdCA).

From E. Bouyer et al. [13].

Table 2
Characterization of Gd-loaded PLGA NPs obtained by W/O/W and W/O/O double-emulsion procedures.

Tableau 2
Caractéristiques des nanoparticules de PLGA incorporant des complexes de Gd obtenues par les procédés de double émulsion W/O/W et W/O/O.

| | PLGA NPs | | | | | |
| | W/O/W | | | W/O/O | | |
GdCAs	D_h (nm)[a]	ζ (mV)[b]	EE (%)[c]	D_h (nm)[a]	ζ (mV)[b]	EE (%)[c]
DOTAREM®	255 ± 10	-27 ± 1	0.66	Flocculation		
Na[Gd(DOTA)]	152 ± 4	-54 ± 3	0.62	256 ± 4	-26 ± 1	1.35
Prohance®	168 ± 1	-42 ± 1	0.38	195 ± 4	-26 ± 1	0.37
Multihance®	192 ± 4	-37 ± 2	0.15	205 ± 2	-26 ± 1	0.23

[a] D_h = mean hydrodynamic diameter.
[b] ζ = zeta-potential.
[c] EE = encapsulation efficiency (eq. (1)).

to avoid GdCAs leakage, by constituting a steric barrier at emulsion interfaces. Attempts were thus undertaken to enhance tensioactive concentration in aqueous phases (to respect NP size requirements, F68® was replaced by Tween®20, [16]) or to add tensioactive (F68®) simultaneously in inner and external aqueous phases as well as in the organic phase (alternative strategies 1 and 2). All these trials led to EE similar to these reported in Table 2 (maximal obtained EE = 0.57%). Without any convincing argument in hand to interpret the discrepancy between Gd and Cu-complex behavior observed in W/O/W double-emulsion-solvent diffusion results, a new protocol based on W/O/O double-emulsion was set up. The underlying idea was to replace the second aqueous phase by an oily one, in order to attenuate the GdCA tropism for the external aqueous phase (in which they are highly soluble), during the solvent diffusion step. Generally, this strategy is very successful to improve encapsulation yields [17]. In order to fulfill biocompatibility requirements, injectable Stelliesters® were used as an oily phase. In internal and external phases, several tensioactive combinations were tested. From NP production yield ($\sim$ 95%) and morphological points of view, best results were obtained using incorporation of Tween®20 in the internal aqueous phase

and Lipoid®S75 (soya lecithin) in the external oily phase O_2. From a GdCA encapsulation point of view, incorporation of DOTAREM® failed (Table 2). For the other GdCAs, ICP-AES titrations allowed detection of Gd inside the NPs but once again, EEs were poor and not significantly higher than EEs obtained with the W/O/W double-emulsion protocol. The objective being to reach higher NP Gd-loadings for a good diagnosis efficacy, designing a radically different approach was necessary in order to improve GdCA sequestration by a polymer matrix. On the basis of the previously obtained results, one should conclude that PLGA matrix was not the best choice to ensure good retention of highly hydrophilic GdCA complexes. This finding was comparable to those reported by Doiron et al., who managed to encapsulate higher Gd-DTPA payloads in bigger PLGA particles but noticed an extremely rapid Gd release once placed under kinetics conditions [18]. To circumvent this issue, the envisaged solution was then to switch the PLGA matrix to a more hydrophilic biocompatible polymer. For this purpose, polysaccharides such as chitosan (CH) [19] and hyaluronic acid [20] were used to constitute the biopolymer matrix (Scheme 2).

The corresponding polysaccharide NPs were synthesized using an ionotropic gelation process [19] (Fig. 2).

a   b
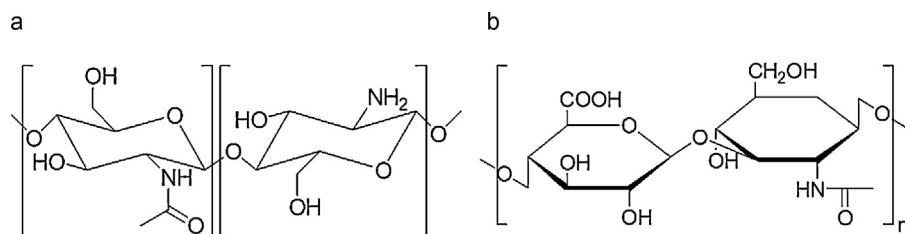
Scheme 2. Hydrophilic polysaccharides (a) chitosan (CH) and (b) hyaluronic acid (HA).
Scheme 2. Polysaccharides hydrophiles (a) chitosane (CH) et (b) acide hyaluronique (HA).
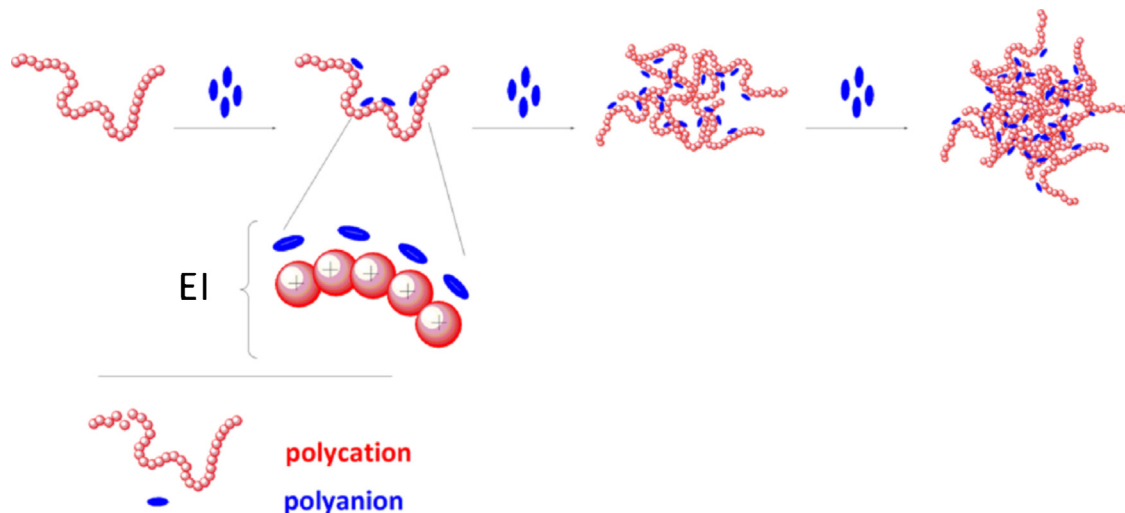

Fig. 2. Schematic representation of ionotropic gelation process (EI for electrostatic interactions).
Fig. 2. Représentation schématique du procédé de gélation ionique (EI pour interactions électrostatiques).

Typically, low-molecular weight chitosan was solubilized in a citric acid solution. In its cationic form, it was allowed to interact with an aqueous solution of polyanions consisting of a mixture of sodium tripolyphosphate (TPP) [21] and sodium hyaluronate (HA) [10]. The formation of inter- and intramolecular electrostatic-mediated cross-linkages between polyanions and protonated chitosan chains spontaneously provoked the gelation process and hydrogel formation. In this respect, hydrogel achievement is very attractive for MRI applications since aqueous environment could be very favorable to relaxivity enhancements. Incorporation of GdCAs in the CH phase allowed the preparation of Gd-loaded NPs (Table 3). The resulting NPs were then purified by dialysis, concentrated by tangential filtration and their content titrated by ICP-AES to determine the encapsulation efficiency and to estimate the number of Gd centers per NP.

To test this strategy several GdCAs were used, linear as well as macrocyclic, neutral as well as charged complexes, for which the counter-ion could be meglumine (for marketed CAs, Scheme 1), sodium ion or proton(s). The rapid examination of EE values showed that for all GdCAs, percentages superior to 1% were systematically reached, which was an improvement compared to previous double-emulsion strategies. However, for DOTAREM®

and Na[Gd(DOTA)], samples were polydisperse (polydispersity indexes superior to 0.3) and mean diameters were superior to what was expected for parenteral uses. For these reasons, these formulations were dismissed. For other GdCAs, NP mean diameters were within the 250 nm range with polydispersity indexes inferior to 0.2, which was suitable for the foreseen applications. Nevertheless, NP production yield remained quite low for Prohance® and

Table 3
Characterization of GdNPs obtained by ionotropic gelation.

Tableau 3
Caractéristiques des GdNPs obtenues par gélation ionique.

GdCAs	D_h[b] (nm)	ζ (mV)[c]	EE (%)[d]	Y_{Gd} ($\times 10^3$)
DOTAREM®	553 ± 3	26 ± 1	1.1	1047
Na[Gd(DOTA)]	300 ± 2	27 ± 1	1.2	187
H[Gd(DOTA)][a]	244 ± 4	45 ± 2	2.9	215
H_2[Gd(DTPA)][a]	241 ± 4	40 ± 2	1.2	87
Prohance®	212 ± 1	29 ± 1	1.1	77
Multihance®	235 ± 3	41 ± 1	1.5	139

[a] H[Gd(DOTA)] and H_2[Gd(DTPA)] correspond to the acidic forms of DOTAREM® and Magnevist® respectively (Scheme 1 for formula).
[b] D_h = mean hydrodynamic diameter.
[c] ζ = zeta-potential.
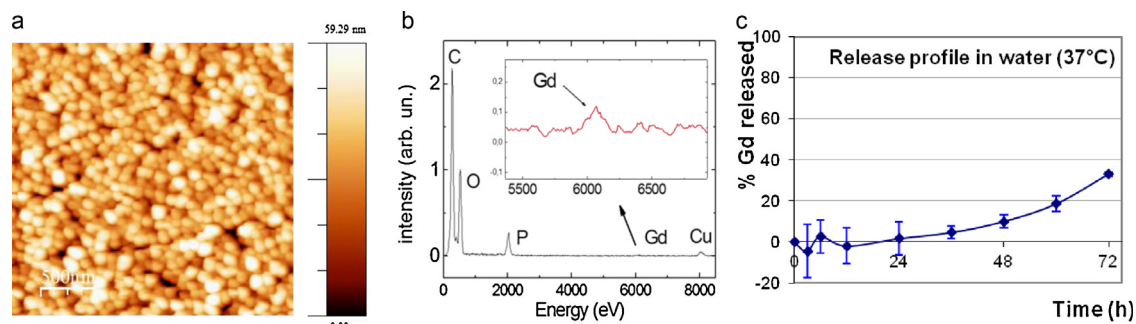[d] EE = encapsulation efficiency [eq. (1)].

Fig. 3. (a) AFM and (b) TEM-EDXS characterizations of H[Gd(DOTA)]⊂NPs. (c) Release profile of H[Gd(DOTA)] at 37 °C in water ([Gd]intraNP = 46 mM).

Fig. 3. Clichés (a) AFM et (b) TEM-EDXS des H[Gd(DOTA)]⊂NPs. (c) Profil de libération de H[Gd(DOTA)] à 37 °C dans l'eau ([Gd]intraNP = 46 mM).
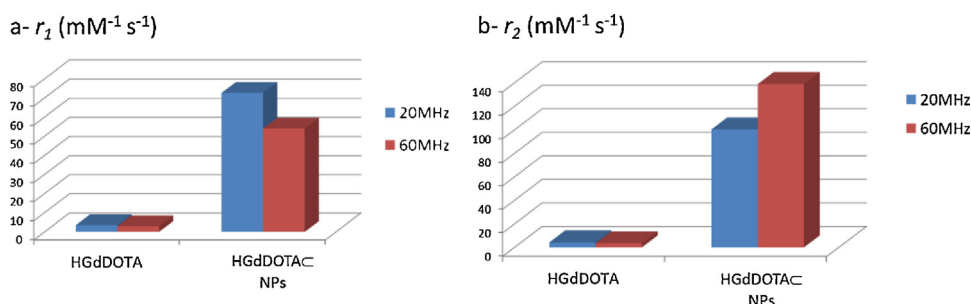

Fig. 4. (a) r_1 and (b) r_2 H[Gd(DOTA)] and H[Gd(DOTA)]⊂NPs relaxivities at 20 MHz (left-hand-side bars) and 60 MHz (right-hand-side bars).

Fig. 4. Relaxivités (a) r_1 et (b) r_2 de H[Gd(DOTA)] et des H[Gd(DOTA)]⊂NPs à 20 MHz (left-hand-side bars) et 60 MHz (right-hand-side bars).

Multihance® contrast agents since production yields inferior to 30% were obtained. For these reasons, these formulations were also dismissed. In fact, with ionic H[Gd(DOTA)] and H2[Gd(DTPA)], better compromises between NP production yield (∼50%) and morphological NP aspects were reached. The improved encapsulation rates were certainly due to electrostatic interactions between the cationic polymer and the anionic complexes. The ionotropic gelation process, driven by electrostatic interactions, appeared then to be a good and simple solution for GdCA encapsulation.

Undoubtedly, the best result was obtained for H[Gd(DOTA)] encapsulation (H[Gd(DOTA)]⊂NPs: EE = 2.9%, average number of Gd-chelates per NP of 2.15×10^5 and subsequent intra-particular Gd concentration of 46 mM). Control experiments were carried out to check if similar H[Gd(DOTA)] loadings could be obtained by simple adsorption or permeation of the complex onto the nanoparticles. Unloaded NPs were incubated with similar H[GdDOTA] amounts and purified in the same way. After purification, no detectable amount of Gd was measured in NP pellets, which confirmed that previous Gd-loadings obtained by ionotropic gelation were not due to adsorption.

AFM experiments showed that H[Gd(DOTA)]⊂NPs were spherical, non-aggregated and homogeneously dispersed (Fig. 3a) [10]. Furthermore, the presence of Gd inside the polymer matrix was confirmed by TEM-EDXS (Fig. 3b).

The release kinetics of the complex included inside the NPs was undertaken in water at 37 °C under sink conditions (Fig. 3c). The release profile indicated that no release of the nanoparticle content occurred at least on the first day. Subsequent release occurred very slowly, reaching less than 40% in 3 days. This behavior, typical for hydrogels, [22] might indicate that in vivo, the loss of the contrast agent pool would be limited even without covalent linkage of the GdCAs to the polymer matrix.

Relaxivity measurements (Fig. 4) indicated that, in comparison to the free complex H[Gd(DOTA)], the particles exhibited very important r_1 and r_2 enhancements (25 − 28 times for r_1 and 32–55 times for r_2 at 20 MHz and 60 MHz respectively) [10][1].

These results can be interpreted on the basis of the geometrical confinement of GdCAs and on the nanoparticle composition. Indeed, inclusion of many Gd complexes inside the hydrophilic matrix can result in a reduction of the CAs rotational tumbling rate and multiple interactions between the exchangeable protons of the water molecules bound to the Gd complexes and the other water molecules confined within the nanoparticle inner-core [23]. All these aspects are in favor of relaxivity exaltation and the resulting system was similar to that obtained with Gd-loaded liposomes [24] or for compartmentalized gadolinium complexes in the apoferritin cavity [25].

Related results were obtained on a 3 T clinical imager where T_1- and T_2-weighted images of phantoms constituted

---

[1] For NMRD profile of H[Gd(DOTA)]⊂NPs see ref [10]. Briefly, a maximum in relaxivity between 25 and 30 MHz was determined for H[Gd(DOTA)]⊂NPs.

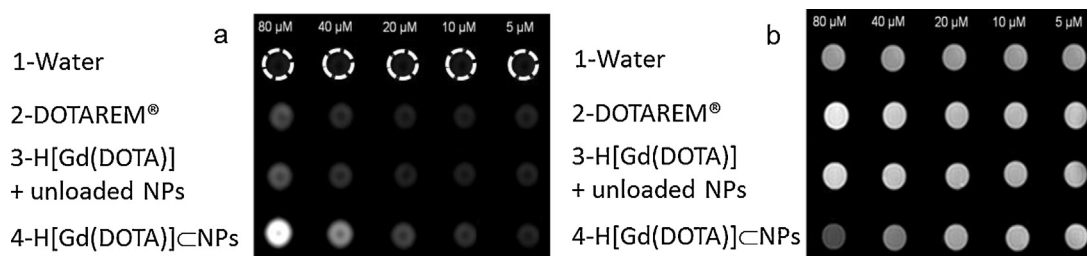**Fig. 5.** (a) T_1-weighted and (b) T_2-weighted MR images of H[Gd(DOTA)]⊂NPs. Water, DOTAREM® and unloaded NPs incubated with H[Gd(DOTA)] were used as controls.

Fig. 5. Images IRM (a) T_1-pondérées et (b) T_2-pondérées des H[Gd(DOTA)]⊂NPs. L'eau, DOTAREM® et des nanoparticules blanches incubées avec du H[Gd(DOTA)] constituent les différents contrôles.

of aqueous suspensions of H[Gd(DOTA)]⊂NPs were performed ([Gd] varying from 5 to 80 µM, Fig. 5). MR images recorded with water and DOTAREM® as controls were simultaneously obtained under same conditions.

For T_1-weighted images, a bright signal enhancement progressively increased with increasing H[Gd(DOTA)]⊂NPs concentration (Fig. 5a, line 4). Phantom containing H[Gd(DOTA)]⊂NPs appeared to be significantly brighter than the two controls (lines 1 and 2). For T_2-weighted images, with same concentration conditions, decreasing signal intensity was observed with increase of H[Gd(DOTA)]⊂NPs concentration (Fig. 5b). To check if these contrast enhancements were correlated to the encapsulation of H[Gd(DOTA)] inside hydrogels, a third control constituted of unloaded NPs (hydrogel without incorporation of GdCA), incubated with increasing identical amounts of H[Gd(DOTA)] was also recorded (line 3). Comparison of lines 4 and 3 demonstrated without any doubt that important contrast enhancements were truly and solely inherent to H[Gd(DOTA)] sequestrated into NPs. These images corroborated therefore relaxation rate results and demonstrated that a good contrast could be obtained with lesser amounts of GdCA. Furthermore, they highlighted the dual properties of the designed NPs since contrast enhancement was observed in both T_1 and T_2 imaging modes.

4. Conclusion

In this paper, encapsulation of marketed MRI GdCAs inside polymeric NPs was carried out through three different protocols for which requirements were similar and based on the sole use of biocompatible materials all along the processes. The two first protocols exploited double-emulsion–solvent diffusion procedures (W/O/W and W/O/O) and PLGA as the polymer matrix. With these techniques, all attempts to reach both high GdCA loadings and acceptable NP production yields failed, whatever the GdCA. These disappointing results prompted us to develop an alternative protocol based on ionotropic gelation. This protocol led to the formation of supramolecular hydrogels in an easy-to-run manner. Biopolymers namely chitosan and hyaluronic acid were used as polymer matrices. Best GdCA incorporation results inside these hydrogels were obtained with H[Gd(DOTA)]. Satisfying NP production yields were reached along with high Gd-loadings. These

high loadings were correlated with the existence of efficient electrostatic interactions between the polymer matrix and the entrapped chelates. Relaxivity measurements and MR images clearly demonstrated that gadolinium-loaded nanoparticles (H[Gd(DOTA)]⊂NPs) exhibited a very efficient ability to enhance T_1 and T_2 – weighted MR images. This might have been related to the occurrence of high concentrations of entrapped GdCAs in a highly hydrated pocket. Therefore, biomaterial-based supramolecular hydrogels turned the clinical widely used GdDOTA into a powerful T_1 and T_2 dual-mode contrast agent. As the complex release from the NPs is very slow, it can be earnestly hypothesized that the NP efficiency concerning the contrast enhancement will last *in vivo* conditions. As a result, these nano-objects represent a noteworthy potential to increase the accuracy of MR imaging for the diagnosis of pathological areas.

Acknowledgements

References

[1] (a) E. Terreno, D. Delli Castelli, A. Viale, S. Aime, Chem. Rev. 110 (2010) 3019 ;
(b) P. Caravan, Chem. Soc. Rev. 35 (2006) 512 ;
(c) A.E. Merbach, E. Toth (Eds.), The Chemistry of Contrast Agents in Magnetic Resonance Imaging, John Wiley and Sons, Chichester, U.K, 2001.
[2] (a) P. Hermann, J. Kotek, V. Kubıcek, I. Lukes, Dalton Trans. (23) (2008) 3027 ;
(b) S. Aime, D. Delli Castelli, S. Geninatti Crich, E. Gianolio, E. Terreno, Acc. Chem. Res. 42 (2009) 822.
[3] N. Bloembergen, L.O. Morgan, J. Chem. Phys. 34 (1961) 842.

[4] C.S. Bonnet, E. Toth, C.R. Chim. 13 (2010) 700.

[5] D.A. Cormode, P.A. Jarzyna, W.J.M. Mulder, Z.A. Fayad, Adv. Drug Deliv. Rev. 62 (2010) 329.

[6] J. Della Rocca, W. Lin, Eur. J. Inorg. Chem. (24) (2010) 3725.

[7] B. Sitharaman, K.R. Kissell, K.B. Hartman, L.A. Tran, A. Baikalov, I. Rusakova, Y. Sun, H.A. Khant, S.J. Ludtke, W. Chiu, W. Laus, E. Toth, L. Helm, A.E. Merbach, L.J. Wilson, Chem. Commun. (31) (2005) 3915.

[8] H.B. Na, T. Hyeon, J. Mater. Chem. 19 (2009) 6267.

[9] (a) T. Courant, V.G. Roullin, C. Cadiou, F. Delavoie, M. Molinari, M.C. Andry, F. Chuburu, Int. J. Pharm. 379 (2009) 226 ;
(b) T. Courant, V.G. Roullin, C. Cadiou, F. Delavoie, M. Molinari, M.C. Andry, V. Gafa, F. Chuburu, Nanotechnology 21 (2010) 165101.

[10] T. Courant, V.G. Roullin, C. Cadiou, M. Callewaert, M.C. Andry, C. Portefaix, C. Hoeffel, M.C. de Golstein, M. Port, S. Laurent, L. Vander Elst, R. Muller, M. Molinari, F. Chuburu, Angew. Chem., Int. Ed. 51 (2012) 9119.

[11] M. Port, J.M. Idée, C. Medina, C. Robic, M. Sabatou, C. Corot, Biometals 21 (2008) 469.

[12] J.L. Grossiord, M. Sellier, STP Pharma. Sci. 11 (2001) 331.

[13] E. Bouyer, G. Mekhloufi, V. Rosilio, J.L. Grossiord, F. Agnely, Int. J. Pharm. 436 (2012) 359.

[14] R.C. Rowe, P.J. Sheskey, in : S.C. Owen (Ed.), Handbook of Pharmaceutical Excipients, 5th edition, Pharm. Press, London, 2005, p. 790.

[15] N. Garti, Colloids Surf. A. 123–124 (1997) 233.

[16] M. Murillo, J.M. Irache, M. Estevan, M.M. Goñi, J.M. Blasco, C. Gamazoc, Int. J. Pharm. 271 (2004) 125.

[17] Y. Li, H.L. Jiang, K.J. Zhu, J.H. Liu, Y.L. Hao, J. Controlled Release 108 (2005) 10.

[18] A. Doiron, K. Chu, A. Ali, L. Brannon-Peppas, Proc. Natl. Acad. Sci. U.S.A. 105 (2008) 17232.

[19] M. Dasha, F. Chiellini, R.M. Ottenbriteb, E. Chiellini, Progr. Polym. Sci. 36 (2011) 981.

[20] F.A. Oyarzun-Ampuero, J. Brea, M.I. Loza, D. Torres, M.J. Alonso, Int. J. Pharm. 381 (2009) 122.

[21] P. Calvo, C. Remuñán-López, J.L. Vila-Jato, M.J. Alonso, J. Appl. Polym. Sci. 63 (1997) 125.

[22] S.A. Agnihotri, N.N. Mallikarjuna, T.M. Aminabhavi, J. Controlled Release 100 (2004) 5.

[23] J.A. Burdick, G.D. Prestwich, Adv. Mater. 23 (2011) H41.

[24] S. Aime, D. Delli Castelli, D. Lawson, E. Tereno, J. Am. Chem. Soc. 129 (2007) 2430.

[25] S. Aime, L. Frullano, S.G. Crich, Angew. Chem., Int. Ed. 41 (2002) 1017.